## Title

Mechanistic in situ insights into the formation, structural and catalytic aspects of the La2NiO4 intermediate phase in the dry reforming of methane over Ni-based perovskite catalysts



## Authors

Nezhad, Parastoo Delir Kheyrollahi
Bekheet, Maged F
Bonmassar, Nicolas
et al.

## Publication Date

2021-02-01

## DOI

10.1016/j.apcata.2020.117984

Peer reviewed

Version of Record: https://www.sciencedirect.com/science/article/pii/S0926860X20305779
Manuscript_efc766a8c2516ab368679af64b6ac78a

# Mechanistic In Situ Insights into the Formation, Structural and Catalytic Aspects of the $La_2NiO_4$ Intermediate Phase in the Dry Reforming of Methane over Ni-based Perovskite Catalysts

Parastoo Delir Kheyrollahi Nezhad[1,2], Maged F. Bekheet[3], Nicolas Bonmassar[2], Lukas Schlicker[3], Albert Gili[3,4], Franz Kamutzki[3], Aleksander Gurlo[3], Andrew Doran[5], Yuanxu Gao,[6] Marc Heggen,[6] Sabine Schwarz[7], Johannes Bernardi[7], Aligholi Niaei[1], Ali Farzi[1], Bernhard Klötzer[2] and Simon Penner[2,*]

[1]*Reactor & Catalyst Research Lab, Department of Chemical Engineering, University of Tabriz, Tabriz, Iran*

[2]*Department of Physical Chemistry, University of Innsbruck, Innrain 52c, A-6020 Innsbruck, Austria*

[3]*Fachgebiet Keramische Werkstoffe/Chair of Advanced Ceramic Materials, Institut für Werkstoffwissenschaften und -technologien, Technische Universität Berlin, Hardenbergstr. 40, 10623 Berlin, Germany*

[4] *Institut für Chemie, Technische Universität Berlin, Sekretariat TC 8, Straße des 17. Juni 124, 10623 Berlin, Germany*

[5]*Advanced Light Source, Lawrence Berkeley National Laboratory Berkeley, California 94720, USA*

[6]*Ernst Ruska-Centrum für Mikroskopie und Spektroskopie mit Elektronen Forschungszentrum Jülich GmbH52425 Jülich, Germany*

[7]*University Service Center for Transmission Electron Microscopy, TU Wien, Wiedner Hauptstrasse 8-10, A-1040 Vienna, Austria*

*Corresponding Author: simon.penner@uibk.ac.at, Tel: 004351250758003, Fax: 004351250758199

**Abstract**

We focus on the stability and bulk/surface structural properties of the Ruddlesden-Popper phase $La_2NiO_4$ and their consequences for dry reforming of methane (DRM) activity. Fuelled by the appearance as a crucial intermediate during in situ decomposition of highly DRM-active $LaNiO_3$ perovskite structures, we show that $La_2NiO_4$ can be equally in situ decomposed into a $Ni/La_2O_3$ phase offering $CO_2$ capture and release necessary for DRM activity, albeit at much higher temperatures compared to $LaNiO_3$. Decomposition in hydrogen also leads to an active $Ni/La_2O_3$ phase. In situ X-ray diffraction during DRM operation reveals considerable coking and encapsulation of exsolved Ni, yielding much smaller Ni crystallites compared to on $LaNiO_3$, where coking is virtually absent. Generalizing the importance of intermediate Ruddlesden-Popper phases, the in situ decomposition of La-based perovskite structures yields several obstacles due to the high stability of both the parent perovskite and the Ruddlesden-Popper structures and the occurrence of parasitic structures.

Keywords: $CO_2$-Activation, B-site Exsolution, Polymorphism, In situ Decomposition

## 1. Introduction

Due to its inherently useful ability of converting the two anthropogenically induced greenhouse gases $CO_2$ and $CH_4$ into useful syngas consisting of $H_2$ and CO, the Dry Reforming of Methane (DRM) reaction

$$CH_4 + CO_2 \rightleftharpoons 2H_2 + 2CO \quad \text{Eq (1)}$$

has attracted a lot of attention in recent years [1-5]. Possible applications exploiting the syngas mixture with $H_2$:CO ratio close to unity, include carbonylation and hydroformylation processes to generate synthetic fuels [6]. Despite the obvious importance, further investigations on mechanistic details, as well as knowledge-driven catalyst development are highly needed, as most catalysts on noble metal basis (e.g., Pd or Ru) are either prohibitively expensive [2, 7-10] or susceptible to coke formation [1-5]. The latter is especially pronounced for the highly active Ni-based systems [11, 12]. Nanoparticulate Ni systems are of particular interest, as they are reported to be more resistant against coke formation [13, 14]. A rather exclusive method to obtain highly dispersed Ni-nanoparticles, which has been in focus for research in various areas of catalytic research, is connected to the exsolution of Ni particles from complex oxide materials, such as perovskites. In essence, Ni is exclusively removed from the B-site of differently doped perovskite materials, mostly upon reductive catalyst treatments. Although many perovskite entities have been used for DRM studies, most information has been compiled on pure and doped La-based perovskite structures. B-site Ni exsolution data from $LaNiO_3$ [5, 15] or layered perovskites (so-called Ruddlesden Popper phases) such as $La_2NiO_4$ [16, 17] are particularly abundant. However, despite the large pile of available data, mechanistic studies are still scarce, and many interpretational ambiguities remain. The latter is due to two reasons: firstly, a pre-reduction treatment in hydrogen is usually conducted prior to the actual DRM reaction to trigger the Ni exsolution. This rises the question of how different gas atmospheres affect the structure of the catalysts, and whether the observed phenomena during DRM reaction or hydrogen reduction can be compared. It has

already been shown by ex situ X-ray diffraction (XRD) studies on La-based perovskite systems that the Ni crystallite/particle size, the effective Ni area, and the formation of the supposedly $CO_2$ activating La-oxy carbonate species are different if the exsolution is triggered in either the DRM mixture or by a pre-treatment in hydrogen. We also note that so far, most mechanistic studies rely purely on ex situ analysis of initial and spent DRM catalyst states. In a recent work on pure and doped La-based perovskite systems, we have shown how the structurally and chemically complex dynamical response of the catalyst in the DRM mixture affects efficient catalyst operation [18]. We observed phase transformations, the formation of oxygen-deficient structures and transient perovskite-related structures upon heating in the DRM mixture and were able to assess their individual importance in the formation of the final active Ni-La-(oxy)carbonate interface, also as a function of doping on the A- and/or B-site of the perovskite structure [18].

As one crucial intermediate, which is formed transiently before observing a significant rise in the catalytic DRM activity, the Ruddlesden-Popper phase $La_2NiO_4$ arises at around 600 °C upon heating $LaNiO_3$ in the DRM mixture. This phase is interesting from multiple viewpoints: it not only appears as an intermediate structure, but is also the most important parasitic phase that is formed when the inherently unstable doped $LaNiO_3$ phase is attempted to be synthesized as phase-pure material. Ex situ XRD and TEM analysis has already revealed a much increased coking propensity of the decomposition products of $La_2NiO_4$ compared to $LaNiO_3$ [16]. Most importantly, we have recently shown that $La_2NiO_4$ is only formed as an intermediary phase if $LaNiO_3$ is heated in the DRM mixture, but not if a pre-reduction is carried out in hydrogen [16]. This suggests that the conditions of La(oxy)carbonate formation (and hence, their interface to exsolved Ni), as well as their structural features are different, again confirming the different dynamic catalyst response and underlining the importance for in situ studies. As literature [16] and our own work [18] thus far indicate that DRM could be in principle equally started from $La_2NiO_4$ instead of from $LaNiO_3$, in turn saving one

preparation step, in this manuscript we focus on the catalytic features of the undoped $La_2NiO_4$ phase and its correlation to the catalyst structure. Of particular importance is answering the question, if the directly synthesized $La_2NiO_4$ phase exhibits a different behavior than the $La_2NiO_4$ phase that is in situ formed during the collapse of the $LaNiO_3$ structure in terms of Ni exsolution, La(oxy)carbonate formation, coking and catalytic performance. To fulfil this task, we rely on the study of (i) unreduced and (ii) pre-reduced $La_2NiO_4$ by applying catalytic tests, in situ X-ray diffraction (XRD) and ex situ X-ray potoelectron spectroscopy (XPS), as well as Transmission Electron Microscopy (TEM) studies. We follow an already well-established pathway of structure-activity correlation, that has previously enabled us to provide essential mechanistic insights into the DRM operation of (doped) perovskite materials [18].

## 2. Experimental

### 2.1. Synthesis of the materials

$La_2NiO_4$ was synthesized following a well-established auto-ignition method [19]. In a first step, an aqueous solution was prepared by mixing stoichiometric amounts of $La(NO_3)_3 \cdot 6\ H_2O$ and $Ni(NO_3)_2 \cdot 6\ H_2O$ in deionized water. Subsequently, glycine was added to the solution in a molar ratio of 1:1 with respect to $NO_3^-$:$NH_2^-$ to induce the formation of glycine-metal complexes, causing a homogeneous distribution of all ions. Excess water was removed upon heating the solution at 80 °C for 2 h. Autothermal self-ignition was triggered by heating the resulting gel to 250 °C at 10 °C $min^{-1}$. Finally, annealing at 900 °C for 12 h yields the $La_2NiO_4$ Ruddlesden-Popper structure (cf. Figure 3). The analoguous synthesis approach was used for (doped) perovskite structures, namely $LaCoO_3$, $LaMnO_3$, $LaCu_{0.3}Mn_{0.7}O_3$ (LCM37) and $LaCu_{0.5}Mn_{0.5}O_3$ (LCM55) using stoichiometric amounts of $La(NO_3)_3 \cdot 6\ H_2O$, $Co(NO_3)_2 \cdot 6\ H_2O$, $Mn(NO_3)_2 \cdot 4\ H_2O$ and $Cu(NO_3)_2 \cdot 3\ H_2O$, respectively and final calcination at 650 °C for 5 h.

2.2. Structural Characterization

The specific surface area prior to catalysis was assessed by BET surface quantification via nitrogen adsorption at 77 K. A Quantachrome Nova2000 surface and pore size analyzer was used for all measurements, yielding BET areas of around 2 $m^2\ g^{-1}$.

Ex situ powder X-ray diffraction (PXRD) was carried out using a STOE Stadi P powder diffractometer operating in transmission geometry and exploiting monochromatized $MoK_{\alpha 1}$ radiation ($\lambda$ = 0.7093Å). A $2\theta$ range of 64° and a step size of 0.015° was used. A focussing Ge(111) primary beam monochromator, as well as a linear position-sensitive detector system was additionally employed.

In situ synchrotron-based PXRD experiments have been conducted in both DRM mixtures and under pure hydrogen at beamline 12.2.2, Advanced Light Source (ALS) at Lawrence Berkeley National Laboratory, in a cell previously described in refs [20, 21]. All diffraction patterns were measured in angle-dispersive transmission mode with a focussed 25 keV monochromatic beam ($\lambda$ = 0.4984Å/30 µm spot size). The powders were heated in a 0.7 mm outer diameter quartz capillary under quasi flowing conditions ($CH_4$:$CO_2$ = 1:1, gas flow: 10:10 mL $min^{-1}$ for DRM; pure hydrogen, gas flow 10 mL $min^{-1}$, GSHV= 600000 $NmL \cdot h^{-1} \cdot g_{cat}^{-1}$). Heating was performed using a SiC furnace with an infrared light source up to 800 °C at a rate of 10 °C $min^{-1}$. All gases were injected through a 0.5 mm outer diameter tungsten tube. The patterns were recorded using a Perkin Elmer flat panel detector (XRD 1621 with dark image and strain correction [20, 21]. Rietveld refinement was performed using the FULLPROF program [22]. The profile function 7 (Thompson-Cox-Hastings pseudo-Voigt convoluted with axial divergence asymmetry function) [23] was used in all refinements. The resolution function of the diffractometers was obtained from the structure refinement of a $LaB_6$ standard.

Surface characterization was performed using X-ray photoelectron spectroscopy (XPS) on a Thermo Scientific MultiLab 2000 spectrometer, equipped with a monochromatic Al Kα X-ray source (E = 1486 eV) and an Alpha 110 hemispherical analyzer. The base pressure lies in $10^{-10}$ mbar range, and charging of the sample upon measurement is compensated by a flood gun supplying electrons with a kinetic energy of 6 eV. The used pass energy was 20 eV. Relevant high-resolution spectra in the relevant La 3d, Ni 2p, and Ni 3p regions have been collected and used for qualitative and quantitative analysis. The latter, with respect to Ni, has been exclusively performed using Ni 3p due to the strong overlap of the La 3d and Ni 2p peaks. After background subtraction using a Shirley-type function, deconvolution of the Ni 3p peak into $Ni^{2+}$ and metallic Ni components was done, obeying the spin-orbit coupling of the individual Ni $3p_{1/2}$ and Ni $3p_{3/2}$ peaks for each relevant component. The full width at half maximum has been fixed for the individual deconvoluted Ni species as an additional constraint. In contrast, the position of the Ni components were left floating to account for the constant change of the Ni chemical environment during decomposition of $La_2NiO_4$.

Structural and morphological characterization has been further performed by ex situ transmission electron microscopy (TEM) using conventional and aberration-corrected microscopes at the *University Service Facility for Transmission Electron Microscopy* (USTEM) at TU Vienna and *Ernst-Ruska Center for Microscopy and Spectroscopy with Electrons* at FZ Jülich, respectively. A FEI Tecnai F20 S-TWIN analytical high-resolution microscope operated at 200 kV in combination with a windowless Apollo XLTW silicon drift detector for EDX experiments was employed to judge sample morphology, geometry and electron diffraction patterns. All aberration-corrected high-resolution TEM experiments were conducted at the FZ Jülich using FEI Titan 80-300 TEM and STEM microscopes operated at 300 kV. Information limits (TEM) of below 90 pm at 300 kV [24] and < 80 pm (at 300 kV; STEM) [25] are obtained.

2.3. Catalytic Testing

The performance of the catalysts with respect to DRM activity was tested in a home-built quartz fixed-bed tubular flow reactor (inner diameter = 7 mm, outer diameter = 9 mm, catalyst bed length: 2.5 cm). Each gas required for DRM ($CH_4$:$CO_2$:He = 1:1:3 ratio; GSHV= 60000 $NmL \cdot g_{cat} \cdot h^{-1}$) was injected through a corresponding mass flow controller (MKS), where helium acts both as a carrier gas and as a heat conductor. 100 mg catalyst powder was used for each test and homogeneously distributed using thoroughly degassed quartz wool over the entire catalyst bed. Heating was achieved using a Linn High Term furnace up to 800 °C at a fixed rate of 10 °C $min^{-1}$. An S-type Pt/PtRh thermocouple placed in close vicinity to the sample ensured accurate temperature reading. The output gas was continuously extracted through a capillary and analyzed by a quadrupole mass spectrometer mounted in cross-beam geometry (Balzers QMA 125). Hydrogen pre-treatments were carried out in 1 bar flowing hydrogen at a rate of 10 mL $min^{-1}$ up to 800 °C.

We especially emphasize here, that due to the bifunctional operating mechanism of DRM catalysts on perovskite basis, normalization of the catalytic activity solely to the surface area of the exsolved Ni particles would grossly overestimate the intrinsic, structure-insensitive catalytic role of Ni and is therefore not considered (i.e., calculating metal surface-based turnover frequencies is not meaningful during in-situ activation). To derive a qualitative understanding and judgment of structure-activity correlations from temperature-programmed DRM experiments, we rely on onset temperatures of catalytic activity, conversion (%) and $H_2$/CO product ratios. The relative catalytic activity is, therefore, compared on the basis of conversion vs. T plots.

## 3. Results and Discussion

The current understanding of catalytic DRM operation on perovskite materials essentially is a bifunctional synergistic action of both metal (mostly Ni [18, 26, 27] but e.g., also Pd [5]) for methane activation and oxide (e.g., $La_2O_3$ in case of perovskite precursors) for $CO_2$ activation. It is currently discussed whether spillover effects or special interfacial sites represent are connected to the active phase. The common structural denominator of all prospective catalyst materials, encompassing not only perovskite-related structures, but also (oxy)carbides or alloy/intermetallic compounds, is the presence of a selected precursor structure, which via in situ decomposition in the DRM mixture or specific forms of pre-activation yields the active metal/oxide material. The latter can be present as $Ni/La_2O_3/La_2O_2CO_3$ (in the case of $LaNiO_3$-based perovskites [18, 26, 27]), $Ni/Mo_2C(WC)$ (in case of carbide materials [28]) or $Pd/ZrO_2$ (in case of Pd-Zr alloys/intermetallic compound precursors [5]).

To focus on the formation of the supposedly active $Ni/La_2O_3/La_2O_2CO_3$ interface from different perovskite precursors (as previous studies suggested vastly different Ni crystallite/particle sizes, a different coking behavior and accordingly, a different catalytic activity starting from different $Ni/La_2O_3$ precursors [16]), we in the following conducted a systematic variation of the experimental parameters to disentangle the individual contributions and its effects on coking, Ni crystallite/particle size, and structural stability of different crystalline phases. The full set of in situ experiments comprises: i) heating up in the DRM mixture starting from unreduced $La_2NiO_4$, ii) conducting a second DRM run starting from the treated catalyst in step i), and iii) heating up in the DRM mixture starting from hydrogen-pre-reduced $La_2NiO_4$.

### 3.1. In situ dynamical bulk structural response of $La_2NiO_4$ during DRM

#### 3.1.1. Starting from unreduced $La_2NiO_4$

Figure 1 reveals that pure $La_2NiO_4$, as its perovskite-related counterpart $LaNiO_3$ [18, 26-30], is prone to decomposition after a DRM experiment up to 800 °C and clear signs of exsolution of Ni as small particles are visible. The distribution of the other elements O and La, as shown by the EDX mapping, remains uniform in the fresh and spent catalysts. While this is also expected from previous studies on $LaNiO_3$ [26, 29-34] and $La_2NiO_4$ [16, 17], the observance of strong coking effects (Figure 1, Panel C) is a clear difference to $LaNiO_3$. Formation of a considerable number of graphitic carbon nanofibers (CNF) or carbon nanotubes (CNT) connected to Ni particles is a frequently observed phenomenon (Figure 2, Panel A). These graphitic structures form due to the decomposition of $CH_4$ on the nickel surface, which produces hydrogen gas and carbon atoms, which dissolve inside the nickel particles. After reaching the limit of solubility, carbon precipitates in the form of graphite, usually lifting the nickel particles in the so called tip-growth model [35]. The drop-like shape of the catalytically acting Ni particle visible in Figure 2, Panel B and C, is a typical example of a growing carbon nanostructure. The observed carbon formation has a direct influence on the self-regenerating reaction of $La_2NiO_4$ during DRM. The reaction of the La(oxy)carbonate with carbon

$$La_2O_2CO_3 + C \rightleftarrows La_2O_3 + 2CO \quad \text{(Eq 2)}$$

is crucial for carbon management on the surface [18, 31, 34]. The removal of surface carbon by oxidation with $CO_2$ was proven to increase the reaction rate of both $CH_4$ and $CO_2$, mitigating the deactivation rate of the catalyst: in other words, cleaning the nickel catalyst surface from carbon is beneficial in terms of catalyst stability for the DRM [36], Encapsulation of the catalytic nickel particles during CNT/CNF growth deactivates the particles and stops the growth mechanism. It has been proven that the high percentage of encapsulated nickel particles after DRM shown by ex situ TEM is most probably produced during cooling of the catalyst after reaction [36, 37]. The carbon dissolved inside the nickel catalyst exsolves due to a decrease of the carbon solubility with temperature during slow

cooling, forming an encapsulating structure that was not present during catalysis [35]. These claims are supported by constant $CH_4$ and $CO_2$ reaction rates and the steady appearance of graphitic carbon during catalysis [36].

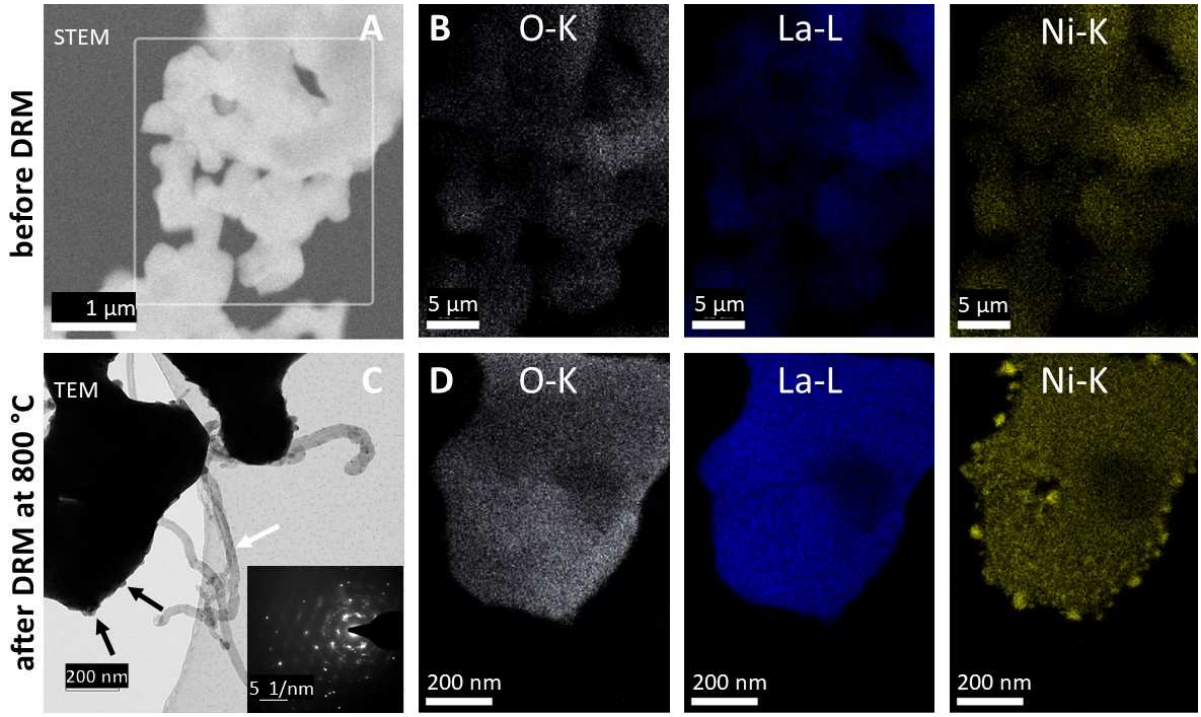


**Figure 1:** (Scanning) transmission electron microscopy analysis of the $La_2NiO_4$ Ruddlesden-Popper phase before (**Panels A and B**), as well as after a catalytic DRM run up to 800 °C (**Panels C and D**). Panels A and C show overview STEM and TEM images, Panels B and D the corresponding EDX analysis. The O-K, La-L and Ni-K intensities are shown, respectively. The inset in Panel C highlights the corresponding SAED pattern after DRM. The black arrows in Panel C indicate the location of two representative exsolved Ni particles (size ~ 25 nm), whereas the white arrow points out the presence of multiwalled carbon nanotubes (MWCNT).

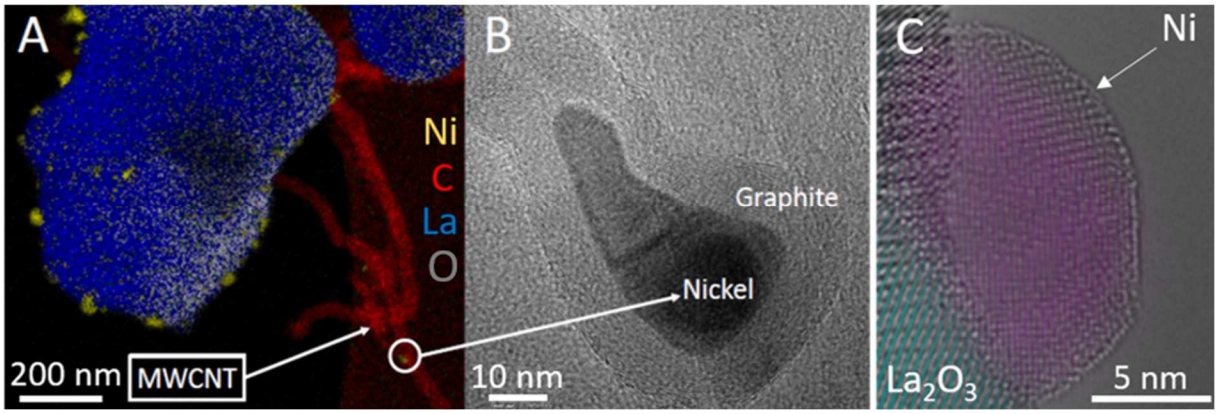


**Figure 2**: **Panel A**: EDX map of the decomposition products of the initial $La_2NiO_4$ structure with exsolved Ni particles after a DRM run up to 800 °C. Ni-K (yellow), C-K (red), La-L (blue), O-K (grey). **Panel B**: High-resolution TEM image of a single detached drop-like Ni particle encapsulated by distorted graphitic carbon layers. The arrow points to the location of the Ni particles at the carbon nanotube. Panel C: High-resolution TEM image of Ni (magenta) and $La_2O_3$ (cyan) after decomposition of $La_2NiO_4$ in the DRM mixture at 800 °C.

Based on previous studies highlighting the importance of evaluation of the dynamic response of the catalyst bulk and surface before and during the DRM treatment for the establishment of valid structure-activity relationships [16, 18], we subjected $La_2NiO_4$ to an in situ XRD treatment in a 1:1 DRM mixture up to 800 °C with an extended isothermal period of 40 minutes at 800 °C. This enables us to follow eventual phase transformations during the heating process, the exsolution of Ni, and the carbon formation more closely.

In summary, the combined analysis outlined in Figures 3-5 reveals several remarkable features of $La_2NiO_4$. At first, a pronounced structural stability of $La_2NiO_4$ during heating in DRM is evident (Figure 3 and Figure 5A). Apart from the phase transformation of minor amounts of parasitic structures such as hydroxylated La-oxide phases in the temperature region 25 °C – 400 °C and the transformation of a $La_2O_3$ stray phase into (oxy)carbonate phases between 450 °C and 800 °C, the $La_2NiO_4$ structure persists decomposition during the heating process (Figure 3 and Figure 5A). This is already in striking contrast to $LaNiO_3$,

where full decomposition during the heating process has been observed [18]. In contrast, we observe several structural transformation during the isothermal period at 800 °C. Figure 4 and Figure 5B reveal three prominent temperature regions with important alterations of structures. In the first region between 0 and 4 minutes, we observe only slight decomposition of $La_2NiO_4$. Accordingly, the amounts of $La_2O_3$, La (oxy)carbonates and exsolved Ni formed are equally low and coking is also not observed within this time frame. The situation changes drastically in the time window between 4 and 7 minutes: here, fast decomposition of $La_2NiO_4$ sets in and within seconds, $La_2NiO_4$ is almost 100 % decomposed with the amount of $La_2O_3$ and metallic Ni rising accordingly. As the experiment is carried out at 800°C and because of the remarkable kinetic metastability of $La_2NiO_4$, the associated structural dynamics of La(oxy)carbonate formation and decay observed for $LaNiO_3$ is not substantially present. Focussing on the evolution of the crystallite size of Ni particles shown in Figure 6 (extracted from the Rietveld refinement), we notice an initial onset crystallite size of around 4.3 nm at 4 minutes, which slightly increases to around 4.5 nm at the time mark of 7 minutes. Most notably, coking is virtually non-existent in this time frame. Only after 7 minutes, coking sets in after the observed induction period, steadily increasing up to 40 minutes. Extrapolating the amount of carbon that is formed during the isothermal period to reaction times beyond 40 minutes suggests saturation at around 50 wt.-%, irrespective of either the amount of Ni or its crystallite size. The latter two, as revealed by Figure 5B and Figure 6, remain stable, and especially, particle sintering is not observed. This behavior can easily be explained on the basis of the TEM images shown in Figure 2B. A considerable amount of Ni particles appear encapsulated in graphitic layers, preventing further sintering.

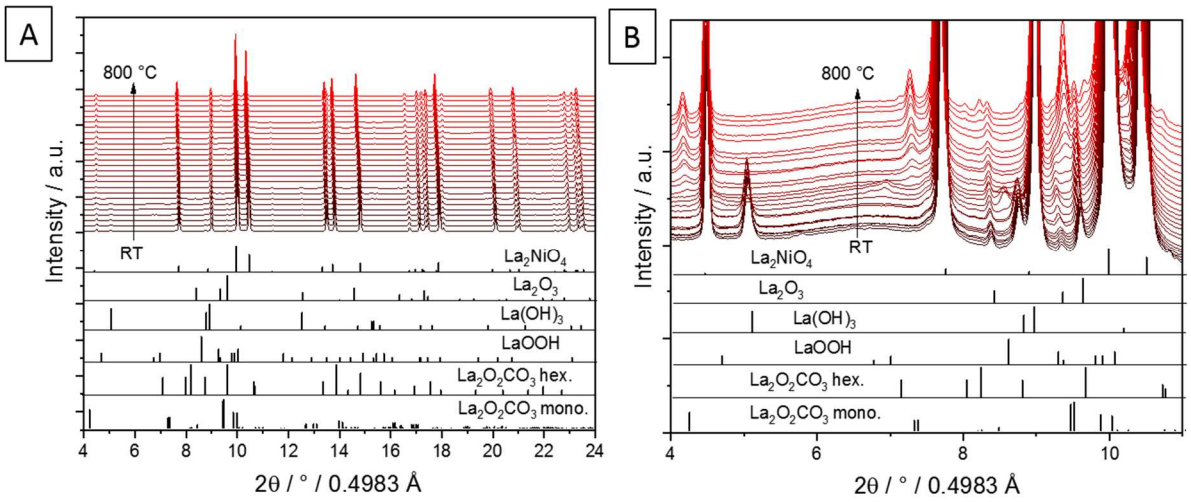


**Figure 3**: **Panel A**: In situ collected XRD patterns of $La_2NiO_4$ during heating up to 800 °C under DRM conditions. **Panel B** focusses on a narrower 2θ window for closer analysis. The lower panel indicates the phase assignment to the respective reference structures.

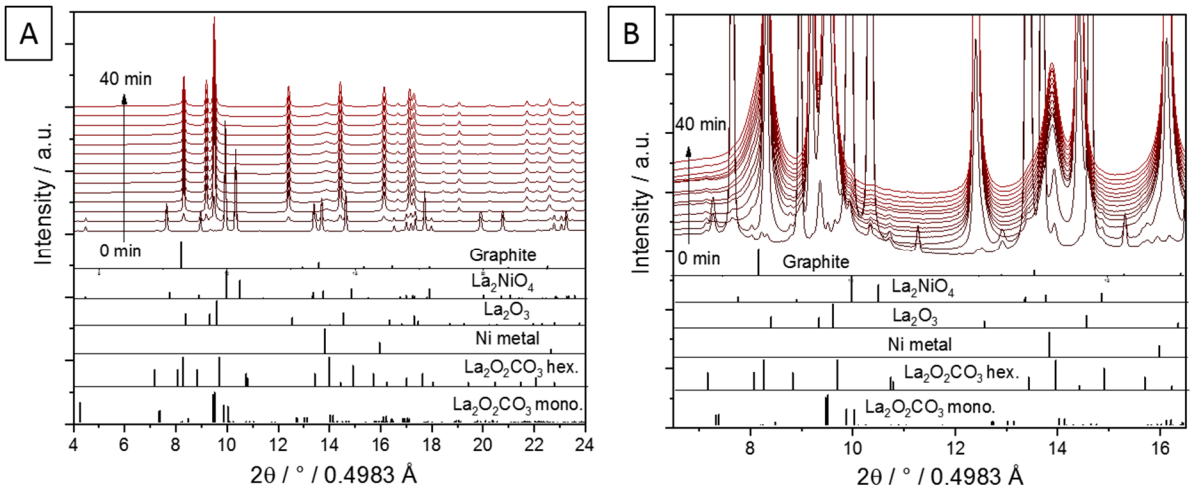


**Figure 4: Panel A**: In situ collected XRD patterns of $La_2NiO_4$ during holding at 800 °C for 40 min under DRM conditions. **Panel B** focus on a narrower 2θ window for closer analysis. The lower panel indicates the phase assignment to the respective reference structures.

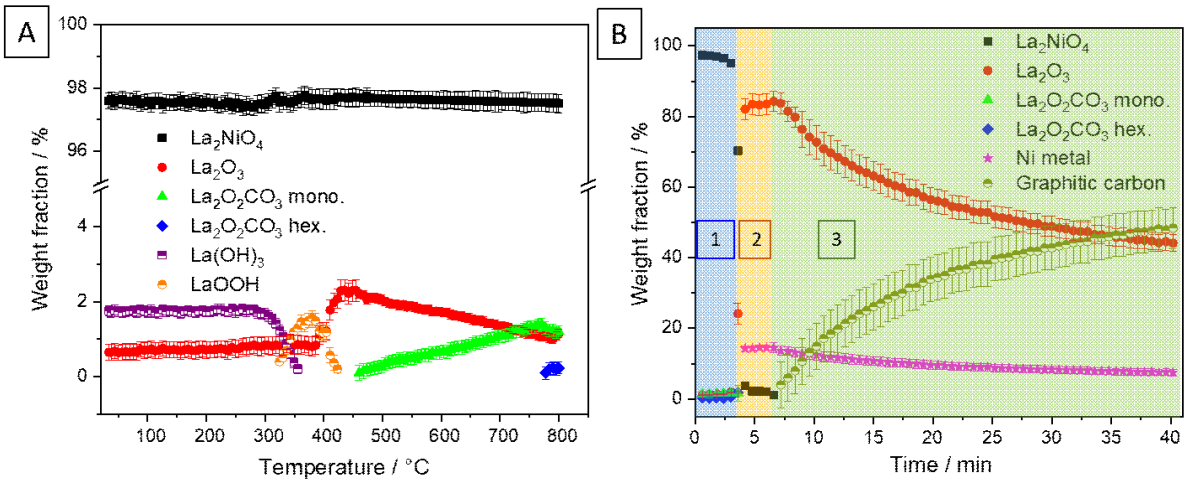


**Figure 5**: Weight fractions of different crystalline phases formed during DRM as a function of temperature (**Panel A**) and time at 800 °C (**Panel B**) obtained by Rietveld refinement of the in situ collected XRD patterns of initial $La_2NiO_4$. The areas marked in Panel B indicate time regions, where significant changes in the participating structures take place, as explained in the main text. Time period 1(blue): 0-4 min; time period 2 (orange): 4-7 min; time period 3 (green): 7-40 min.

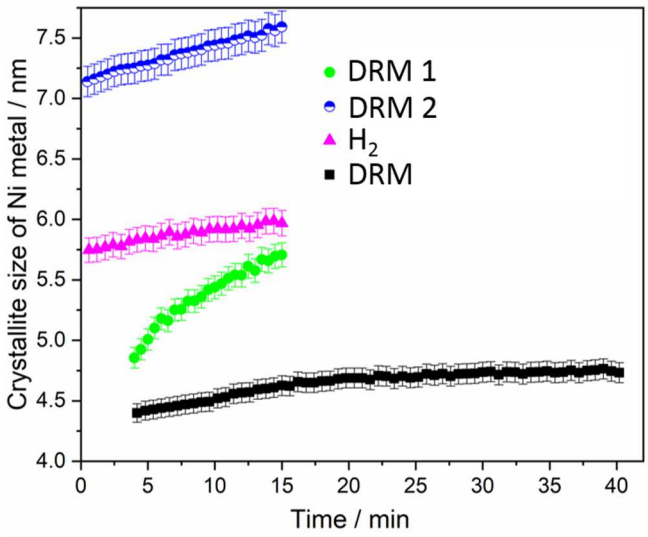


**Figure 6**: Evolution of the crystallite size of exsolved metallic Ni formed during DRM at 800 °C as a function of time as obtained by Rietveld refinement of the in situ collected XRD patterns after selected treatments. Black: decomposition in a $CO_2$:$CH_4$ 1:1 mixture (data extracted from experiment shown in Figure 5B); Magenta: decomposition in hydrogen (data extracted from experiment shown in Figure 7D); Green: decomposition in a $CO_2$:$CH_4$ 1:1

mixture (cycle 1, “DRM 1”); Blue: decomposition in a $CO_2$:$CH_4$ 1:1 mixture (cycle 2, “DRM 2”). “DRM 1” and “DRM 2” refer to an additional experiment with two subsequent individual DRM cycles starting from initally unreduced $La_2NiO_4$ (data extracted from experiment shown in Figure S2).

The results of the second DRM experiment conducted by heating the catalyst in two runs up to 800 °C for 15 min without pre-reduction are presented in Figure S1 (in situ XRD patterns) and Figure S2 (weight fraction analysis). Figure 6 also highlights the corresponding variation of the crystallite size of the metallic Ni particles formed during the experiment with time. Briefly, the qualitative features are quite similar to the ones discussed in the context of Figure 3-5. In the second run of this experiment, the $CO_2$ capture – release cycle via $La_2O_3$ decomposition/formation of monoclinic $La_2O_2CO_3$, intertransformation of monoclinic and hexagonal $La_2O_2CO_3$ and the final decompositon of the $La_2O_2CO_3$ species into $La_2O_3$ at 800 °C is clearly visible in the heating process (Figure S1 panel C and Figure S2 panel D). In the subsequent isothermal phase, the catalyst reaches the steady state conditions quickly with respect to weight fractions of formed $La_2O_3$, Ni and graphitic carbon phases as well as the crystallite size of the metallic Ni phase. The evolution of metallic Ni is essentially predictable, as most of the Ni particles still remain encapsulated and, thus, do not contribute to the catalytic activity.

3.1.2. Starting from hydrogen pre-reduced $La_2NiO_4$

In close correlation to similar experiments on the parent $LaNiO_3$ perovskite, where clear differences both in the in situ-determined structural transformations, as well as the catalytic performance, have been observed starting from fully oxidized or hydrogen pre-reduced $LaNiO_3$ [18], the corresponding experiments on $La_2NiO_4$ after hydrogen pre-reduction show comparable differences. Figure 7 and 8 summarize the results of the

qualitative and quantitative structural evolution during the pre-reduction step and during a subsequent DRM run. Up to 450 °C during pre-reduction, we observe the transformation of minor $La(OH)_3$ into LaOOH and further into $La_2O_3$. The decomposition of $La_2NiO_4$ into $La_2O_3$ and Ni metal occurs in a single and fast step at 550 °C. Moreover, the crystallite size of metallic Ni derived from Rietveld refinement (~ 6 nm), which does not increase remarkably with time, is slightly larger than that of metallic Ni formed in the first experiment ( in situ activation under DRM conditions) without the pre-reduction step in $H_2$ (~ 4.5 nm). As with all other experiments, these results suggest slight Ni particle sintering during the period past the Ni metal formation process. In essence, before the catalytic DRM treatment, the catalyst contains hexagonal $La_2O_3$ in contact with metallic Ni particles composed of ~ 6 nm-sized crystallites. During the DRM treatment (structural evolution Figures 7 Panel C and D, as well as Figure 8, Panel B), in the temperature region between 500 °C and 750 °C, we observe a cycle of $La_2O_3$ carbonation to monoclinic $La_2O_2CO_3$ followed by re-decomposition into $La_2O_3$. The amount of exsolved Ni is apparently constant during the course of DRM reaction. Within the subsequent 15 min isothermal period at 800 °C, coking occurs by graphite formation, in close correlation to the experiments without $H_2$ pre-reduction (Figure S3).

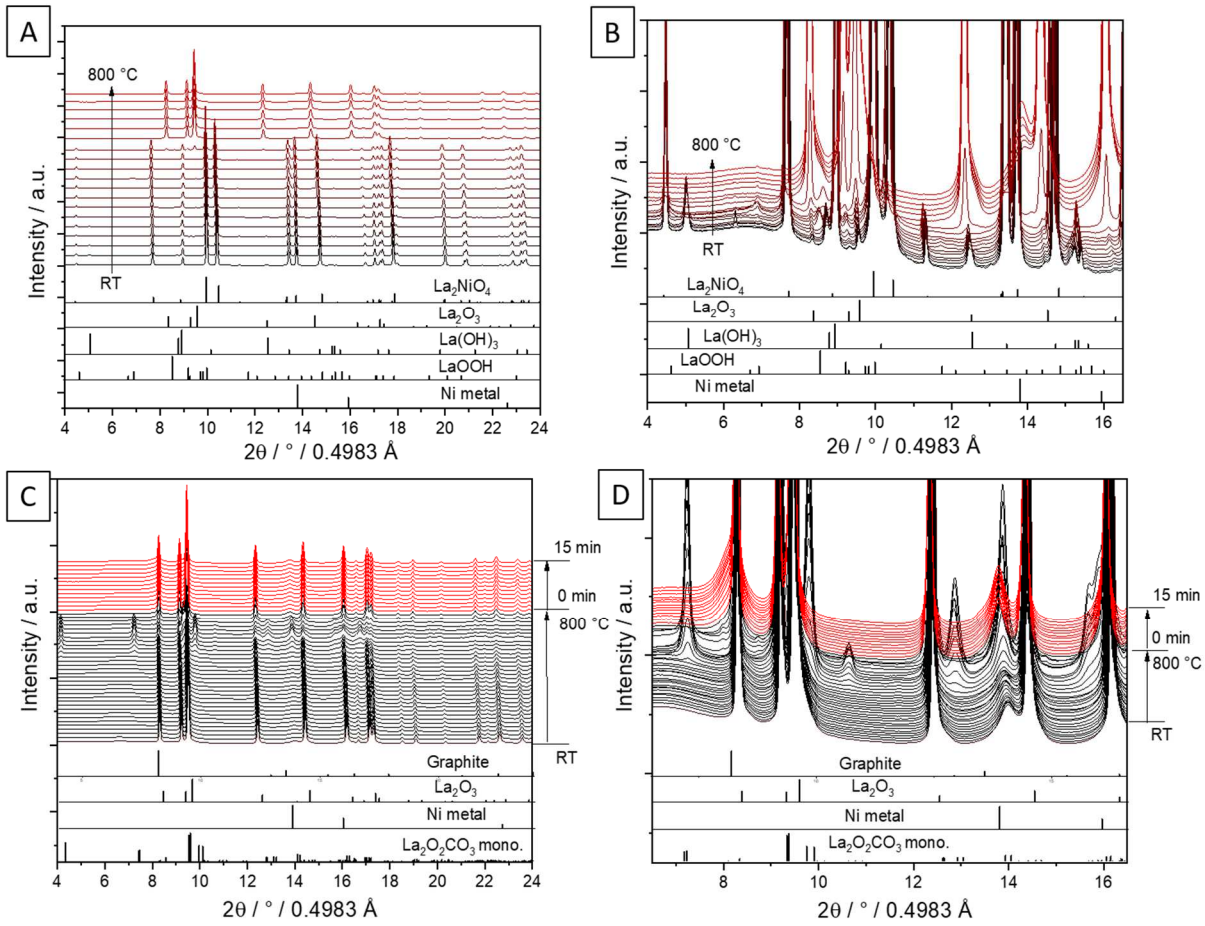


**Figure 7: Panels A** and **B :** In situ collected XRD patterns of initial $La_2NiO_4$ during heating up to 800 °C under $H_2$ conditions. **Panels C** and **D -** In situ collected XRD patterns of already pre-activated $Ni/La_2O_3$ during heating up to 800 °C under DRM conditions with an isothermal period of 15 min after pre-reduction in $H_2$ at 800 °C. **Panels B** and **D** focus on a narrower 2θ window for closer analysis. The lower panels indicate the phase assignment to the respective reference structures.

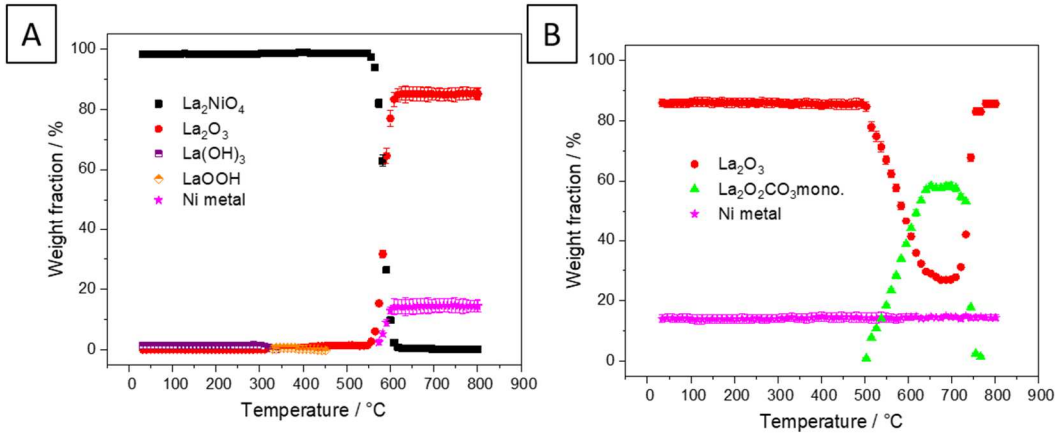

**Figure 8**: Weight fractions of different crystalline phases formed during heating $La_2NiO_4$ in $H_2$ up to 800 °C (**Panel A**), followed by another heating step under DRM conditions up to 800 °C (**Panel B**) as a function of temperature.

It is well known that the methane dry reforming reactivity of $La_2NiO_4$ catalyst precursors could be influenced by orthorhombic – tetragonal phase transformation occurring at around 150 °C and the loss of the interstitial oxygen from the tetragonal structure above 450 °C upon annealing [18]. These structural transitions or chemical expansion of the catalyst at high temperatures is evident from the evolution of the lattice parameters and the unit cell volume. Figure S4 shows a comparative assessment of the evolution of the cell parameters *a*, *b* and *c* with temperature for the four catalyst samples heated under DRM and $H_2$ atmosphere. The annotations $a_o$, $b_o$, as well as $a_t$, $b_t$ refer to the lattice parameter of the orthorhombic and tetragonal structures, respectively. Rietveld refinement reveals that the $La_2NiO_4$ catalyst precursor exhibits an orthorhombic *Fmmm* structure at room temperature, which agrees with previous reports [18]. Upon heating, the cell parameters $a_o$ and $b_o$ of the orthorhombic $La_2NiO_4$ (converted through a $\sqrt{2}a$ relationship to a tetragonal cell) converge at 125 and 175 °C under DRM and $H_2$ conditions, respectively, indicating the orthorhombic-to-tetragonal (*I*4/*mmm* structure) transformation. This result agrees with previous in situ neutron diffraction studies reporting the irreversible orthorhombic-to-tetragonal transformation of $La_2NiO_4$ at about 150 °C [18]. Our experiments showed that the orthorhombic-tetragonal transformation is shifted to lower temperature under $H_2$ atmosphere, which can be explained by the increase in reducibility in $H_2$ if compared with DRM, thus, supporting the formation of tetragonal oxygen-depleted phases at lower temperatures. With a further increase in the temperature, there is a clear chemical expansion observed in the temperature ranges 230-380 °C and 450-650 °C under under $H_2$ and DRM, respectively. This expansion is accompanied by a sharp decrease in the *c* parameter and an increase in the *a* parameter, which can be explained by the

loss of excess oxygen occupying the interstitial sites located in the La-O plane in the *ab* direction of the tetragonal lattice. The loss of these interstitial oxygen atoms leads to a compression along the *c* direction and an expansion in the *ab* direction [38, 39]. Thus, this structure transformations occurs at a lower temperature range under $H_2$ atmosphere, which facilitates oxygen loss from the $La_2NiO_4$ lattice upon heating. These results are in good agreement with previous studies showing that the onset temperatures of these two phase transformations of $La_2NiO_4$ depends on the gas atmosphere [40].

For a more detailed quantitative analysis, the weight ratio of the $La_2O_3$/Ni and $La_2O_2CO_3$/Ni active phases observed on the in-situ DRM activated vs. the $H_2$-activated catalysts (at 800 °C for 15 min) and on a pristine $LaNiO_3$ reference sample are calculated from Rietveld refinement results. As shown in Figure 9, the pretreated $La_2NiO_4$ samples exhibit a Ni/$La_2O_3$ composite as the respective active phases below 500 °C. Above 500 °C, the $La_2O_2CO_3$/Ni ratio increases, while the $La_2O_3$/Ni ratio decreases until a steady state composition is attained in the temperature range 600-790 °C and 630-730 °C for the initial $La_2NiO_4$ samples pretreated either in DRM or $H_2$, respectively. Similarly, $La_2O_2CO_3$/Ni composites as active phases are observed for $LaNiO_3$ samples only up to ~750 °C. After passing through this steady state, the $La_2O_2CO_3$/Ni ratio decreases again, while the $La_2O_3$/Ni ratio increases. These results suggest that the steep rate increase observed for the three in-situ and the $H_2$-activated catalysts in the temperature range 550-750 °C (Figure 8 for $La_2NiO_4$, [18] for $LaNiO_3$) is associated with the simultaneous presence of the $La_2O_2CO_3$/Ni composite. In due course, the diminished conversion increase around ~ 750 °C can be assigned to the transformation of $La_2O_2CO_3$ into the $La_2O_3$ phase. This finding points out that the $La_2O_2CO_3$/Ni composite is most likely more active towards the methane dry reforming than any $La_2O_3$/Ni composite.

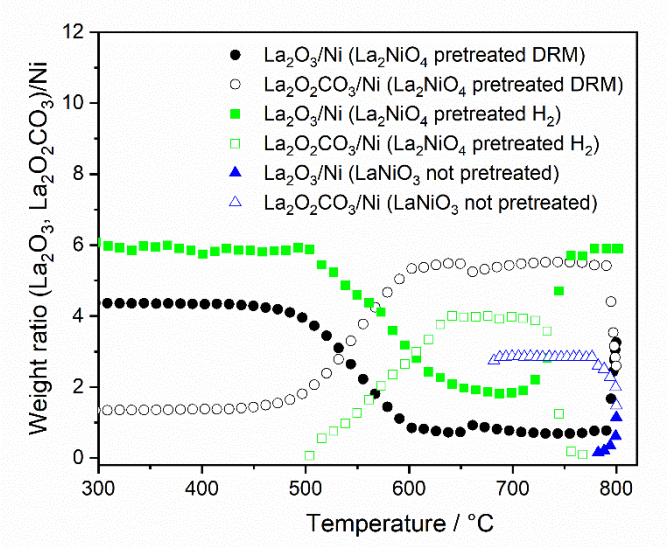


**Figure 9:** Weight ratio of $La_2O_3$/Ni (filled symbols) and $La_2O_2CO_3$/Ni (hollow symbols) phases formed upon heating in DRM of $La_2NiO_4$ pretreated in DRM (circles) and $H_2$ (squares) at 800 °C for 15 min. For comparison, the associated data obtained on untreated $LaNiO_3$ (triangles) are also shown.

3.1.3. Surface characterization by XPS

The chemical state of the elements and the surface composition of the catalysts was revealed by XPS analysis of the $La_2NiO_4$ treated under different conditions (Figure 10 and Table 1). Panel A of Figure 10 shows the spectra of the La 3d + Ni 2p region. Generally, the Ni 2p spectra are very complex due to the strong overlap of Ni 2p and La 3d peaks. Thus, in order to investigate the surface characteristics more clearly, the Ni 3p spectral range (Figure 10, Panel B) was chosen for analysis instead. In essence, the chemical trend already derived from bulk XRD analysis is corroborated. Before the catalytic DRM treatment, the whole Ni 3p spectrum can - as expected - be fitted using a single oxidic Ni ($Ni^{2+}$) component, while hydrogen pre-reduced $La_2NiO_4$ clearly shows an increased amount of exsolved metallic Ni. A metallic Ni component was also observed upon a direct DRM experiment up to 800 °C *without* $H_2$ pre-reduction. However, as expected, this amount is much lower. Starting a DRM cycle from Ni/$La_2O_3$ (arising either from $H_2$ pre-reduction or in situ DRM decomposition of

$La_2NiO_4$) increases the amount of surface-bound metallic Ni even further. A word of caution should be added at this point with respect to the observed $Ni^{2+}$ component after any indicated treatment. As it follows from the XRD results discussed above, complete decomposition of the initial $La_2NiO_4$ structure occurs after any of the treatments discussed in Figure 4 and 8 with quantitative tranformation of Ni to its metallic state. The observed $Ni^{2+}$ component therefore arises from contact to ambient conditions via tranfer to the XPS chamber. The discussed qualitative trends, nevertheless, remain unaffected by this apparent contradiction.

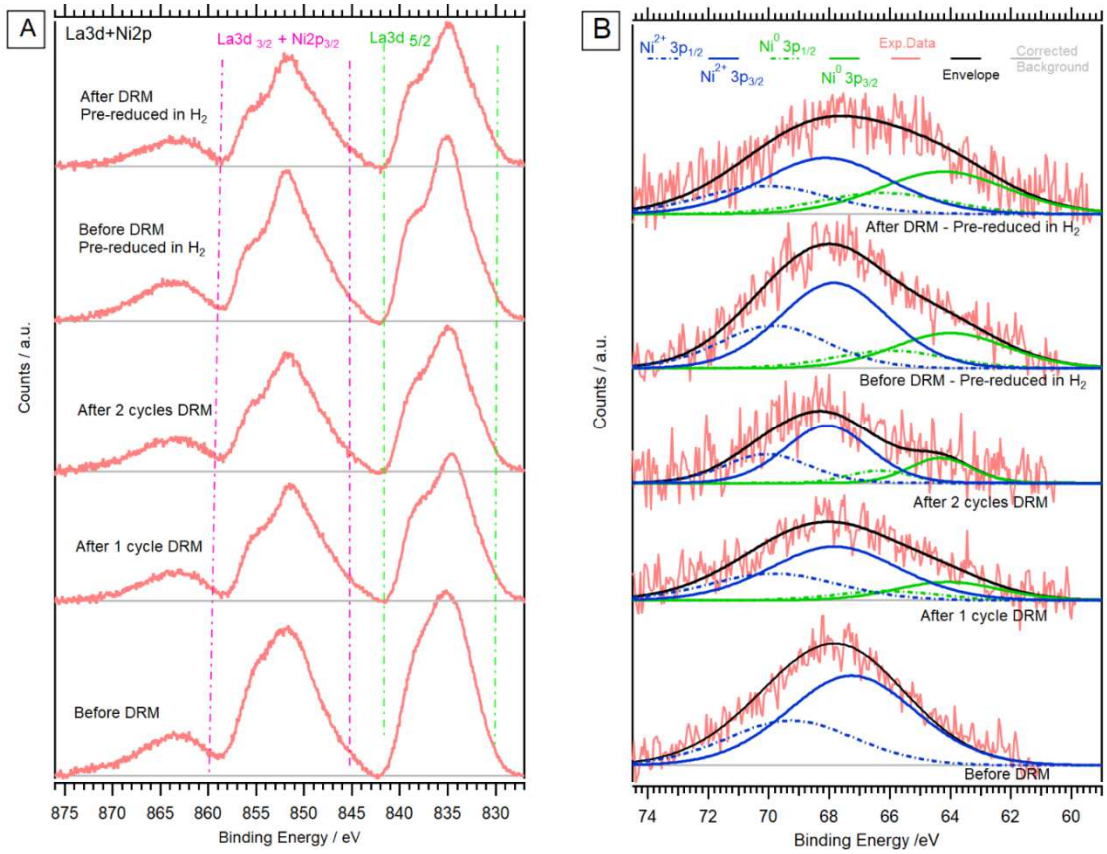


**Figure 10:** Ex-situ X-ray photoelectron spectra collected on $La_2NiO_4$ after selected oxidative and reductive pre-treatments, as well as after several catalytic DRM runs. **Panel A**: La 3d and Ni 2p region, **Panel B**: Ni 3p region. A Shirley-type background correction and deconvolution into $Ni^{2+}$ (blue traces) and metallic Ni components (green traces) have been performed as outlined in the experimental section.

**Table 1**: Quantitative analysis of the Ni 3p region after selected catalyst pre-treatments and catalytic DRM runs. Amounts are given in at.-%.

| Catalyst ($La_2NiO_4$) | Ni $3p_{3/2}$ ($Ni^{2+}$) | Ni $3p_{3/2}$ ($Ni^0$) |
|---|---|---|
| Before DRM | 100 | - |
| After 1 cycle DRM | 78.16 | 21.84 |
| After 2nd cycle DRM – started from 1st cycle DRM treated catalyst | 68.26 | 31.74 |
| Reduced with $H_2$ | 64.12 | 35.88 |
| After DRM – started from pre-reduced catalyst with $H_2$ | 57 | 43 |

3.1.4. Catalytic profiles in DRM

Figure 11 displays the catalytic profiles obtained on $La_2NiO_4$ after selected oxidative and reductive pre-treatments. the pre-reduction in hydrogen at 800 °C for 30 min – to obtain the active $Ni/La_2O_3$ phase – has a tremendously beneficial effect on the catalytic performance, as shown by the increase in both $CH_4$ and $CO_2$ conversion over the whole temperature range compared to the unreduced sample. The onset temperature of catalytic DRM activity is shifted by ~120 °C to lower temperatures for both for the $H_2$-prereduced catalyst and the DRM in-situ activated catalyst. In fact, the profiles of the latter almost match, which suggests lack of substantial deactivation and that the bulk and surface structure of the active phase after pre-reduction in hydrogen and after in situ DRM activation, both including a 30 min isothermal period at 800 °C, is comparable as corroborated by both in situ XRD and XPS. The $H_2/CO$ ratios (depicted as inset in Figure 11), obtained during a DRM run after $H_2$ pre-reduction (magenta-colored trace), during a second DRM reaction after a first DRM cycle (blue trace), are close to unity over the reaction time period above 700 °C. During the first DRM cycle without pre-reduction in hydrogen (green trace) in the activation period between 700 °C and

800 °C, the $H_2$/CO ratio increases and finally reaches a value close to unity at 800 °C, as expected.

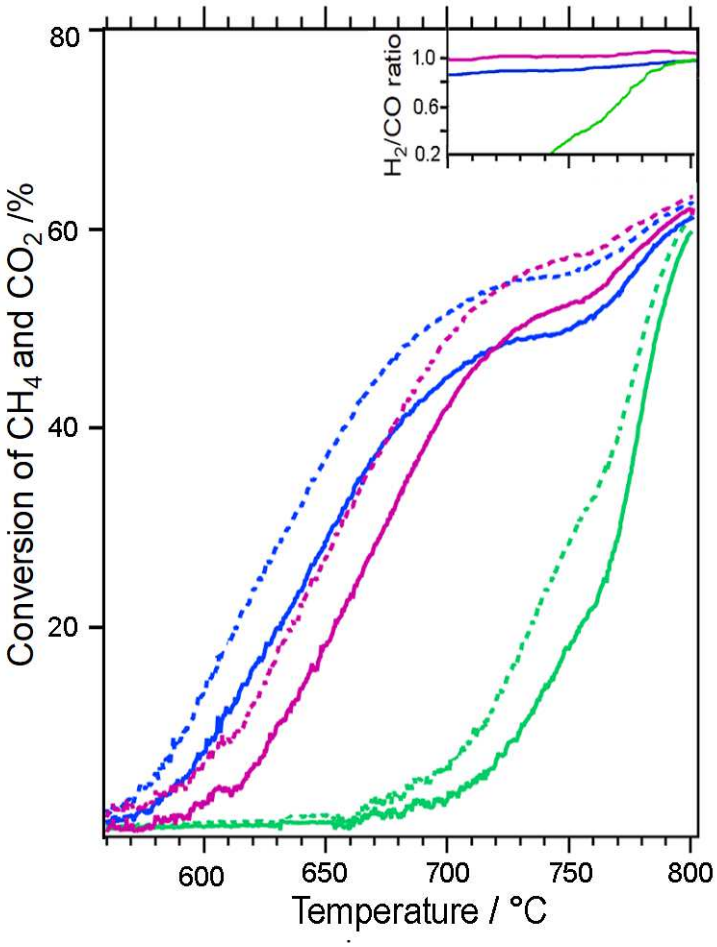


**Figure 11:** Catalytic DRM profiles displayed as carbon dioxide (broken lines) and methane conversion (full lines) on $La_2NiO_4$ after selected oxidative (calcination at 900 °C for 12 h) and reductive pre-treatments (reduction in $H_2$ flow diluted with He with heating rate of 10 °C $min^{-1}$ including isothermal period at 800 °C for 30 min). Color code: magenta - $La_2NiO_4$ with pre-reduction in $H_2$; green - $La_2NiO_4$ without pre-reduction 1st DRM cycle; blue - $La_2NiO_4$ without pre-reduction 2nd DRM cycle. The $H_2$/CO ratio for selected catalytic profiles is shown as inset. Experimental conditions: $CH_4$:$CO_2$:He = 1:1:3 fixed at 100 mL $min^{-1}$. Heating was performed up to 800 °C at a rate of 10 °C $min^{-1}$.

3.1.5. Discussion

We will separate the discussion basically into two parts: at first, a direct relation to the intrinsic properties of the parent $LaNiO_3$ perovskite will yield the potential importance of the $La_2NiO_4$ intermediate phase. Secondly, we will put our results into literature perspective to discuss eventual similarities and differences in catalytic operation. Especially for the latter, a pile of mostly ex situ works already exists, that allows to more efficiently interpret the in situ data [16, 18, 28-34].

In comparison with $LaNiO_3$ [18], $La_2NiO_4$ is structurally much more stable in the DRM mixture. While $LaNiO_3$ starts to form sub-stoichiometric perovskite structures by the release of lattice oxygen already around 520 °C, inducing Ni exsolution at ~ 600 °C [18], $La_2NiO_4$ remains stable up to 800 °C. However, the decomposition of $La_2NiO_4$ occurs on a much shorter time scale in a single step within minutes in contrast to $LaNiO_3$, where the decompositon starts at much lower temperatures and proceeds over a temperature region of at least 150 °C. The evolution of the crystallite size of metallic Ni formed upon decomposition of both materials reveals a much larger crystallite size at 800 °C for $LaNiO_3$ compared to $La_2NiO_4$ (~ 8 nm vs. ~ 4.5 nm), which can be understood on the basis of on a prolonged sintering process for Ni particles exsolved from $LaNiO_3$. Equally important for the catalytic DRM operation is the ability to enable a (oxy)carbonate formation/release cycle [18]. In this respect, the reversible formation, transformation and decomposition of monoclinic and hexagonal $La_2O_2CO_3$ phases accompanying the Ni exsolution appears to better accomplished on initial $LaNiO_3$. We suggest that both the required self-regeneration cycle and, via the high abundance of activated $CO_2$ at the Ni-oxycarbonate phase boundary, the efficient suppression of coking via the reverse Boudouard reaction $CO_2(g) + C(s) \leftrightarrows 2CO(g)$ [18] work better on in-situ DRM-activated $LaNiO_3$. Both of these requirements are not satisfactorily fulfilled on $La_2NiO_4$: due to its pronounced structural stability up to 800 °C (above the temperature stability limit of the La(oxy)carbonate species), the self-regeneration cycle via

La(oxy)carbonate formation/decomposition is essentially suppressed and coking is apparently an issue, as the clean-off process via the reverse Boudouard reaction cannot proceed.

To understand the role of intermediate $La_2NiO_4$ during the catalytic DRM process on initial $LaNiO_3$, we note that upon a hydrogen pre-reduction treatment, the decomposition temperature of $La_2NiO_4$ is decreased to 550 °C. This is exactly the temperature region, where the DRM activity on $LaNiO_3$ is strongly accelerated, indicating that hydrogen formed through the limited DRM activity of the $LaNiO_{2.7}$ and $LaNiO_{2.5}$ phases between 520 °C and 620 °C, triggers and facilitates the decomposition of $La_2NiO_4$. The small temperature offset in the decomposition temperature (550 °C on initial $La_2NiO_4$ in 1 bar pure hydrogen vs. 620 °C for in situ formed $La_2NiO_4$ during the DRM process on initial $LaNiO_3$) can be understood on the basis of the smaller reaction-induced hydrogen partial pressure in the DRM mixture for in situ formed $La_2NiO_4$, decreasing the reduction rate. In this respect, we can also understand the missing $La_2NiO_4$ phase during hydrogen reduction of initial $LaNiO_3$: as the decomposition of $La_2NiO_4$ in pure hydrogen takes place at much higher temperature (550 °C) than the decomposition of $LaNiO_{2.7}$/$LaNiO_{2.5}$ to Ni/$La_2O_3$ (310 °C, cf. Figure 9 in ref. [18]), these phases decompose in a single step without the intermediate occurrence of $La_2NiO_4$.

Putting our results into literature perspective, we note a particular work by Gallego et al. [16], which deals with carbon dioxide reforming of methane over $La_2NiO_4$ also in comparison with $LaNiO_3$ (essentially based on ex situ analysis), serving as a meaningful scientific base to discuss the findings of our work. In relation to this work, we note several similarities and differences. At first, we note a much higher structural stability of $La_2NiO_4$ in our work (total decomposition at 800 °C only during the isothermal treatment vs. partial already at 700 °C, 1 h; total decomposition after 15 h [16]). This apparent discrepancy might be explained by the smaller grain size of the $La_2NiO_4$ materials used in ref. [16], facilitating faster decomposition. Coking is pronounced in both works upon treatment in the DRM mixture. With respect to the (oxy)carbonate self-regeneration cycle, La (oxy)carbonate

formation is clearly visible in ref. [16]. In our work, the (oxy)carbonate formation is substantially suppressed due to the higher reaction temperature and the associated quick pass beyond of the stability limit of $La_2NiO_4$. However, monoclinic $La_2O_2CO_3$ is the dominant modification in both works. Monoclinic $La_2O_2CO_3$ is apparently of prime importance for the carbonate self-regeneration cycle on both $LaNiO_3$ and $La_2NiO_4$. The behavior upon hydrogen reduction is similar with respect to decomposition temperature (550 °C) and crystallite size of metallic Ni (~ 6 nm).

3.1.6. General importance of Ruddlesden-Popper phases in the catalytic DRM performance of perovskite catalysts

The proven importance of the $La_2NiO_4$ intermediate phase during the catalytic performance of $LaNiO_3$ directly raises the question if this concept can be generalized to similar perovskite systems. Especially La-based single perovskite materials are well-known to exhibit considerable DRM activity, mostly, but not limited to Ni- and Co-doping on the B-site [18, 30, 32-34, 41-47]. In principle, each metallic dopant that can be exsolved from the B site upon either hydrogen reduction or contact to the DRM mixture and which subsequently allows for efficient methane activation, would be a prospective candidate. Provided an associated Ruddlesden-Popper phase, i.e., a catalyst couple $ABO_3/A_2BO_4$, exists, and their respective stability limits are approached within the accessible and technically relevant DRM temperature region, the sequence of $ABO_3 \dashrightarrow A_2BO_4 \dashrightarrow B/A_xO_y$ could be observed. Among the possible catalyst materials, pure and doped perovskites on $LaCoO_3$ and $LaMnO_3$ basis have been screened for DRM or methane/carbon dioxide activation [48-50], as well as pre-reduction in hydrogen to trigger the B-site exsolution.

In the case of $LaCoO_3$ (trigonal structure), pre-reduction triggered the phase transformation to orthorhombic $La_2CoO_4$, as evidenced by in situ X-ray diffraction [51]. As with studies on $LaNiO_3$, analysis is mainly based on ex situ analysis of the initial and spent

catalyst and in situ studies during DRM are non-existent. In order to eventually transfer the ideas of $LaNiO_3/La_2NiO_4$ to similar prospective materials, we performed ex situ structural characterization and catalytic screening tests of $LaCoO_3$, $LaMnO_3$, $LaCu_{0.3}Mn_{0.7}O_3$ and $LaCu_{0.5}Mn_{0.5}O_3$ to evaluate if decomposition in the DRM mixture at 800 °C and catalytic DRM activity are observed. The results are summarized in Figure 12. X-ray diffraction reveals the successful synthesis of all materials (Panel B). Moderate activity in terms of hydrogen and carbon monoxide formation (Figure 12, Panel A) is especially observed for the B-site Cu doped manganite materials, although on both at much higher temperatures compared to $LaNiO_3$ and without any $H_2$/CO stoichiometry that is close to unity. The reason for the - with respect to the Ni-based materials - comparably low DRM activity is obvious from X-ray analysis of the spent catalysts, which reveals no decomposition into a particularily active metal-oxide system after contact with the DRM mixture at least up to 800 °C. Anyway, potential Cu exsolution would not allow for comparable methane activation properties in comparison to metallic Ni. Trigonal $LaCoO_3$ indeed shows transformation to orthorhombic $La_2CoO_4$ and CoO, but with no promotional effect on the DRM performance, as no Co metal is formed. $LaMnO_3$ reveals only a polymorphic transformation from a rhombohedral to an orthorhombic structure. Both $LaCu_{0.3}Mn_{0.7}O_3$ and $LaCu_{0.5}Mn_{0.5}O_3$ reveal partial decomposition into $La_2CuO_4$ and $LaMnO_3$, in addition to the initial perovskite lattices. Potentially explaining their obvious DRM activity, formation of $La_2O_2CO_3$ is also observed – indicating that the activation of $CO_2$ via an active carbonate formation/decomposition cycle required for DRM activity may be at least partially working.

In summary, the structural prerequisites to address the respective Ruddlesden-Popper phases are obviously not satisfactorily fulfilled for the chosen perovskite materials, giving rise to only inferior catalytic properties compared to Ni-based perovskite/Ruddlesden Popper counterparts.

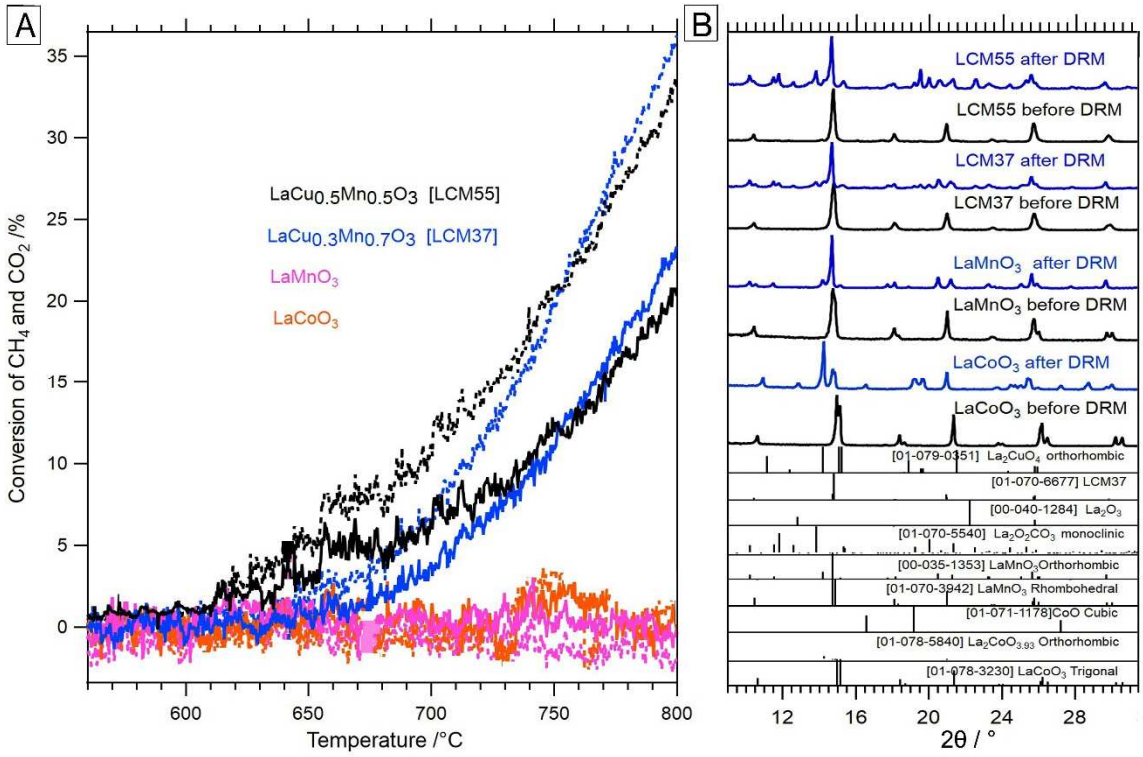


**Figure 12:** Catalytic profiles (displayed as carbon dioxide (broken lines) and methane (full lines) conversion in the methane dry reforming reaction (**Panel A**) on different pure and doped perovskite phases ($LaCoO_3$, $LaMnO_3$, $LaCu_{0.3}Mn_{0.7}O_3$ (LCM37) and $LaCu_{0.5}Mn_{0.5}O_3$ (LCM55)) with known intermediate Ruddlesden-Popper phases. (**Panel B**): X-ray diffraction patterns of the respective perovskite phases before and after DRM reaction. In the DRM experiments ($CH_4$:$CO_2$:He = 1:1:3) the gas mixture flow was fixed at 100 mL $min^{-1}$ and heating was performed up to 800 °C at a rate of 10 °C $min^{-1}$.

## 4. Conclusions

By a comparative approach of the parent $LaNiO_3$ perovskite and the associated Ruddlesden-Popper structure $La_2NiO_4$ using in situ X-ray diffraction and catalytic characterization in the dry reforming of methane reaction, we were able to elucidate the structural stability, intrinsic DRM properties and the central role of the latter in the transition from $LaNiO_3$ via $La_2NiO_4$ into the active Ni/$La_2O_3$/La(oxy)carbonate state. $La_2NiO_4$ thereby shows strikingly different features than its parent $LaNiO_3$ perovskite counterpart, if the

isolated structures are compared. $La_2NiO_4$ exhibits remarkable kinetic metastability in the DRM mixture up to 800 °C. Consequently, its sudden decay counteracts the (oxy)carbonate – based self-regeneration cycle by $CO_2$ capture and CO release. Therefore, the decomposition of $La_2NiO_4$ yields mainly a $Ni/La_2O_3$ composite, which exhibits only limited catalytic activity and pronounced coking propensity at comparable temperatures. In hydrogen, the structural stability is limited, but still higher compared to $LaNiO_3$ (decomposition temperature 550 °C vs. ~ 310 °C). Exactly the observed temperature range for decomposition in hydrogen explains the distinct correlation of decomposition of reaction-formed $La_2NiO_4$ and strong acceleration of product formation in the DRM experiment starting from $LaNiO_3$. As the sub-stoichiometric $LaNiO_x$ phases formed from $LaNiO_3$ (being observable before $La_2NiO_4$ occurs) exhibit moderate DRM activity, the reaction-formed hydrogen aids the decomposition of $La_2NiO_4$ at lower temperatures.

An attempt to generalize the importance of intermediate Ruddlesden-Popper phases in the in situ decomposition of La-based perovskite structures yields several inconsistencies, mainly due to i) a too high stability of the parent perovskite lattice (excluding e.g. $LaMnO_3$), ii) the high stability of the Ruddlesden-Popper structure (eventually blocking reductive Co metal formation and thus excluding $LaCoO_3$ as a catalyst precursor) and, mainly for doped structures, iii) the occurrence of stray structures (excluding e.g. $LaCu_{0.5}Mn_{0.5}O_3$, as it essentially decomposes into $La_2CuO_4$ and $LaMnO_3$). Hydrogen reduction prior to DRM catalysis to obtain the catalytically active metal-oxide material remains then the preparation approach of choice to access prospective DRM catalysts on perovskite basis.

## 5. Acknowledgments

S. Penner acknowledges funding from the Austrian Science Fund (FWF) within the SFB project F4503-N16 “Functional Oxide Surfaces and Interfaces” and the DACH project I2877-N34. The work was performed within the framework of the research platform

“Materials- and Nanoscience” and the special PhD program “Reactivity and Catalysis” at the University of Innsbruck. The authors further thank the Advanced Light Source (which is supported by the Director, Office of Science, Office of Basic Energy Sciences, of the U.S. Department of Energy under Contract No. DE-AC02-05CH11231), where in situ XRD measurements were conducted at beamline 12.2.2 in the framework of the AP program ALS-08865.

**References**

[1] Z. Zuo, S. Liu, Z. Wang, C. Liu, W. Huang, J. Huang, P. Liu, ACS Catal. 8 (2018) 9821–9835. https://doi.org/10.1021/acscatal.8b02277

[2] Global Carbon Project. Surge in Methane Emissions Threatens Efforts To Slow Climate Change. https://phys.org/news/2016-12-surge-methane-emissions-threatens-efforts.html, 2016 (accessed12 December, 2016)

[3] Y. Wang, L. Yao, Y. Wang, S. Wang, Q. Zhao, D. Mao, C. Hu, ACS Catal. 8 (2018) 6495–6506. https://doi.org/10.1021/acscatal.8b00584

[4] S. Arora, R. Prasad, RSC Ad 6 (2016) 108668–108688. https://doi.org/10.1039/C6RA20450C

[5] N. Köpfle, T. Götsch, M. Grünbacher, E. A. Carbonio, M. Hävecker, A. Knop-Gericke, L. Schlicker, A. Doran, D. Kober, A. Gurlo, S. Penner, B. Klötzer, Angew Chem. Int. Ed Engl. 57 (2018) 14613–14618. https://doi.org/10.1002/anie.201807463

[6] R. Franke, D. Selent, A. Börner, Chem Rev. 112 (2012) 5675–5732. https://doi.org/10.1021/cr3001803

[7] J. Kehres, J.G. Jakobsen, J.W. Andreasen, J.B. Wagner, H. Liu, A. Molenbroek, J. Sehested, I. Chorkendorff, T. Vegge, J. Phys. Chem. C 116 (2012) 21407–21415. https://doi.org/10.1021/jp3069656

[8] C. Carrara, J. Múnera, E.A. Lombardo, L.M. Cornaglia, Topics in Catalysis 51 (2008) 98-106. https://doi.org/10.1021/ie061621p

[9] D. Pakhare, J. Spivey, Chem. Soc. Rev. 43 (2014) 7813–7837. https://doi.org/10.1039/C3CS60395D

[10] P. Ferreira-Aparicio, C. Márquez-Alvarez, I. Rodríguez-Ramos, Y. Schuurman, A. Guerrero-Ruiz, C. Mirodatos, J. Catal. 184 (1999) 202–212. https://doi.org/10.1006/jcat.1999.2439

[11] D. Zambrano, J. Soler, J. Herguido, M. Menéndez, Top Catal. 62 (2019) 456–466. https://doi.org/10.1007/s11244-019-01157-2

[12] Q.L.M. Ha, U. Armbruster, C. Kreyenschulte, H. Atia, H. Lund, H.T. Vuong, S. Wohlrab, Catal. Today 334 (2019) 203–214. https://doi.org/10.1016/j.cattod.2018.11.021

[13] M. Akri, S. Zhao, X. Li, K. Zang, A.F. Lee, M.A. Isaacs, W. Xi, Y. Gangarajula, J. Luo, Y. Ren, Y.T. Cui, L. Li, Y. Su, X. Pan, W. Wen, Y. Pan, K. Wilson, L. Li, B. Qiao, H. Ishii, Y.F. Liao, A. Wang, X. Wang, T. Zhang, Nat. Commun. 10 (2019) 1-10. https://doi.org/10.1038/s41467-019-12843-w

[14] J.W. Han, C. Kim, J.S. Park, H. Lee, Chem. Sus. Chem. 7 (2014) 451–456. https://doi.org/10.1002/cssc.201301134

[15] S. Singh, D. Zubenko, B.A. Rosen, ACS Catal. 6 (2016) 4199–4205. https://doi.org/10.1021/acscatal.6b00673

[16] G. Sierra Gallego, F. Mondragón, J.M. Tatibouët, J. Barrault, C. Batiot-Dupeyrat, Catal. Today 133 (2008) 200–209. https://doi.org/10.1016/j.cattod.2007.12.075

[17] M. Wang, T. Zhao, M. Li, H. Wang, RSC Adv. 7 (2017) 41847–41854. https://doi.org/10.1039/C7RA08422F

[18] N. Bonmassar, M. F. Bekheet, L. Schlicker, A. Gili, A. Gurlo, A. Doran, Y. Gao, M. Heggen, J. Bernardi, B. Klötzer, S. Penner, ACS Catal. 10 (2020) 1102-1112. https://doi.org/10.1021/acscatal.9b03687

[19] Pechini, M.P. Method of Preparing Lead and Alkaline Earth Titanates and Niobates and Coating Method Using the Same to Form a Capacitor. (1967) US Patent No. 3330697.

[20] A. Doran, L. Schlicker, C.M. Beavers, S. Bhat, M.F. Bekheet, A. Gurlo, Rev. Sci. Instrum. 88 (2017) 13903-1–13903-6. https://doi.org/10.1063/1.4973561

[21] L. Schlicker, A. Doran, P. Schneppmüller, A. Gili, M. Czasny, S. Penner, A. Gurlo, Rev. Sci. Instrum. 89 (2018) 33904-1-33904-4. https://doi.org/10.1063/1.5001695

[22] Rodriguez-Carvajal, J. Recent Developments of The Program FULLPROF, In Commission on Powder Diffraction (IUCr), Newsletter 26 (2001) 12–19.

[23] L.W. Finger, D.E. Cox, A.P. Jephcoat, J. Appl. Crystallogr. 27 (1994) 892-900. https://doi.org/10.1107/S0021889894004218

[24] A. Thust, J. Barthel, K. Tillmann, FEI Titan 80-300 TEM. J. Large-Scale Facilities 2 (2016) A41. https://doi.org/10.17815/jlsrf-2-66

[25] M. Heggen, M. Luysberg, K. Tillmann, FEI Titan 80-300 STEM, J. Large-Scale Facilities 2 (2016) A42. https://doi.org/10.17815/jlsrf-2-67

[26] S. Kühl, H. Düdder, F. Girgsdies, K. Kähler, M. Muhler, M. Behrens, J. Inorganic and General Chem. 643 (2017) 1088–1095. https://doi.org/10.1002/zaac.201700141

[27] S. Royer, D. Duprez, F. Can, X. Courtois, C. Batiot-Dupeyrat, S. Laassiri, H. Almdari, Chem. Rev. 114 (2014) 10292-10368. https://doi.org/10.1021/cr500032a

[28] Z. Yao, J. Jiang, Y. Zhao, F. Luan, J. Zhu, Y. Shi, H. Gao, H. Wang, RSC Adv. 6 (2016) 19944-19951. https://doi.org/10.1039/C5RA24815A

[29] J.J. Juan, M.C. Roman-Martınez, M.J. Illan-Gomez, Appl. Catal. A 355 (2009) 27–32. https://doi.org/10.1016/j.apcata.2008.10.058

[30] C. Batiot-Dupeyrat, G. Valderrama, A. Meneses, F. Martinez, J. Barrault, J. Tatibouët, Appl. Catal. A 248 (2003) 143–151. https://doi.org/10.1016/S0926-860X(03)00155-8

[31] C. Batiot-Dupeyrat, G.A.S. Gallego, F. Mondragon, J. Barrault, J.M. Tatibouët, Catal. Today 107-108 (2005) 474 – 480. https://doi.org/10.1016/j.cattod.2005.07.014

[32] G.R. Moradi, F. Khosravian, M. Rahmanzadeh, Chin. J. Catal. 33 (2012) 797–801. https://doi.org/10.1016/S1872-2067(11)60378-1

[33] F. Touahra, A. Rabahi, R. Chebout, A. Boudjemaa, D. Lerari, M. Sehailia, K. Bachari, Int. J. Hydrogen Energy 41 (2016) 2477–2486. https://doi.org/10.1016/j.ijhydene.2015.12.062

[34] J.L.G. Fierro, J.M.D. Tascón, L.G. Tejuca, J. Catal. 93 (1985) 83-91. https://doi.org/10.1016/0021-9517(85)90153-8

[35] A. Gili, L. Schlicker, M.F. Bekheet, O. Görke, D. Kober, U. Simon, P. Littlewood, R. Schomäcker, A. Doran, D. Gaissmaier, T. Jacob, S. Selve, A. Gurlo, ACS Catalysis, 9 (2019) 6999-7011. https://doi.org/10.1021/acscatal.9b00733

[36] A. Gili, L. Schlicker, M.F. Bekheet, O. Görke, S. Penner, M. Grünbacher, T. Götsch, P. Littlewood, T.J. Marks, P.C. Stair, R. Schomäcker, A. Doran, S. Selve, U. Simon, A. Gurlo, ACS Catalysis, 8 (2018) 8739-8750. https://doi.org/10.1021/acscatal.8b01820

[37] S. Hofmann, R. Sharma, C. Ducati, G. Du, C. Mattevi, C. Cepek, M. Cantoro, S. Pisana, A. Parvez, F. Cervantes-Sodi, A.C. Ferrari, R. Dunin-Borkowski, S. Lizzit, L. Petaccia, A. Goldoni, J. Robertson, Nano Letters, 7 (2007) 602-608. https://doi.org/10.1021/nl0624824

[38] S. J. Skinner, Solid State Sci 5 (2003) 419-426. https://doi.org/10.1016/S1293-2558(03)00050-5

[39] A. Aguadero, J. A. Alonso, M. J. Martinez-Lope, M. T. Fernandez-Diaz, M. J. Escudero, L. Daza, J Mater Chem 16 (2006), 3402-3408. https://doi.org/10.1039/B605886H

[40] M. T. Fernandez-Diaz, J. L. Martinez, J. Rodriguez-Carvajal, Solid State Ionics, 1993, 63-65, 902-906. https://doi.org/10.1016/0167-2738(93)90213-M

[41] H. Arandiyan, J. Li, L. Ma, S.M. Hashemnjad, M.Z. Mirzaei, J. Chen, H. Chang, C. Liu, C. Wang, L. Chen, J. Ind. Eng. Chem. 18 (2012), 2103-2114. https://doi.org/10.1016/j.jiec.2012.06.004

[42] G. Valderrama, A. Kiennemann, C.U. de Navarro, M. Goldwasser, Appl. Catal. A 565 (2018), 26-33. https://doi.org/10.1016/j.apcata.2018.07.039

[43] G. Valderrama, A. Kiennemann, M.R. Goldwasser, Catalysis Today 133-135 (2008) 142-148. https://doi.org/10.1016/j.cattod.2007.12.069

[44] T. Wei, L. Jia, H. Zheng, B. Chi, J. Pu, J. Li, Applied Catalysis A: General 564 (2018) 199-207. https://doi.org/10.1016/j.apcata.2018.07.031

[45] E. P. Komarala, I. Komissarov, B.A. Rosen, Catalysts 10 (2020) 27. https://doi.org/10.3390/catal10010027

[46] T.V. Sagar, D. Padmakar, N. Lingaiah, K.S. Rama Rao, I.A.K. Reddy, P.S. Sai Prasad, J. Chem. Sci. 129 (2017), 1787–1794. https://doi.org/10.1007/s12039-017-1359-2

[47] A. Tsoukalou, Q. Imtaz, S.M. Kim, P.M. Abdala, S. Yoon, C.R. Müller, J. Catal. 343 (2016), 208-214. https://doi.org/10.1016/j.jcat.2016.03.018

[48] K.T.C. Roseno, R. Brackmann, M.A. da Silva, M. Schmal, Intl. J. Hydrogen Energy 41 (2016) 18178-18192. https://doi.org/ 10.1016/j.ijhydene.2016.07.207

[49] M. de Santana Santos, R. Crisostomo Rabelo Neto, F. Bellot Noronha, P. Bargiela, M. da Graca Carneiro da Rocha, C. Resini, E. Carbo-Argibay, R. Frety, S. Teixeira Brandao, Catal. Today 299 (2018), 229-241. https://doi.org/10.1016/j.cattod.2017.06.027

[50] X. Wang, Y. Liu, Y. Zhang, T. Zhang, H. Chang, Y. Zhang, L. Jiang, Appl. Catal. B 229 (2018) 52-62. https://doi.org/10.1016/j.apcatb.2018.02.007

[51] S. Ortatli, J. Ternieden, C. Weidenthaler, Eur. J. Inorg. Chem. 48 (2018) 5238-5245. https://doi.org/10.1002/ejic.201801162

**TOC Graphic**

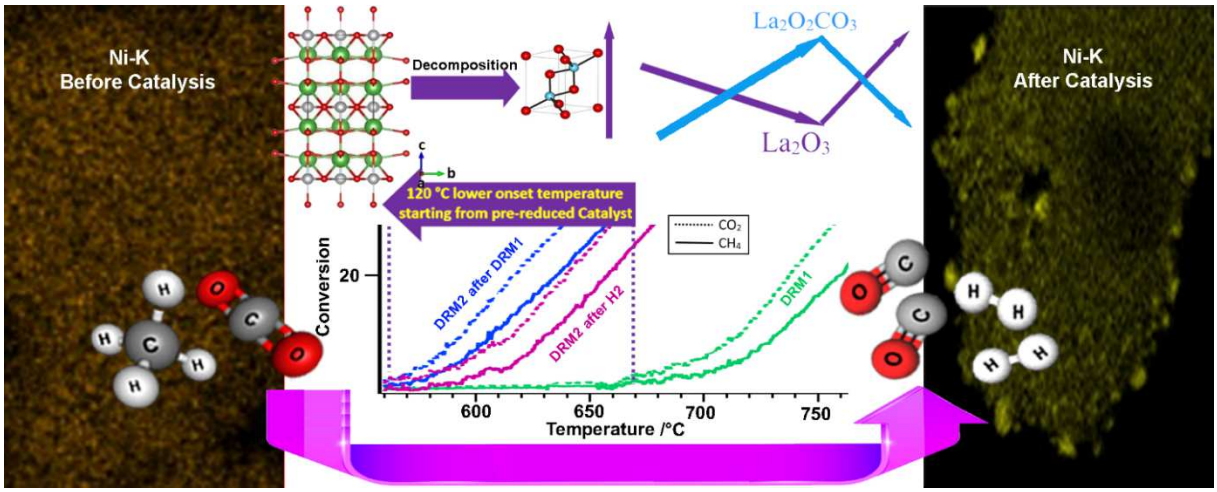
Ni-K
Before Catalysis
Decomposition
$La_2O_2CO_3$
$La_2O_3$
Ni-K
After Catalysis
120 °C lower onset temperature
starting from pre-reduced Catalyst
$CO_2$
$CH_4$
Conversion
20
DRM2 after DRM1
DRM2 after H2
DRM1
600
650
700
750
Temperature /°C